Recent advances in the aerodynamic design of steam turbine components

R. Greim, S. Havakechian
ABB Alstom Power, Baden, Switzerland

Summary

This paper addresses two major issues, which are believed to have significant impact on the design of advanced steam turbines. The first issue concern automation and modernization of the existing design tools applied mainly for the conventional balding flow path design. Further, substantial CFD modeling efforts on turbine components besides standard blading flow path, are discussed to indicate areas of potential aerodynamic loss reduction and practical solutions, which lead to additional performance improvement.

Notation

ΔH	Stage static enthalpy drop
U_m	Mean rotor circumferential velocity
C_x	Axial velocity at the mean radius
ν	Flow coefficient (C_x / U_m)
μ	Stage loading (ΔH / U_m^2)
R	Stage degree of reaction (ΔH_{rotor} / ΔH)

1 Introduction

Today's requirements of advanced steam turbine design place special emphasis on the design simplicity, fewer parts, enhanced reliability and maintainability. Such requirements, when coupled with the ever-increasing demand on the higher efficiency level for both existing and new design concepts, offer the most challenging problem to the design engineers.
Modern turbine-design entails integrated program system, which accounts for many of the above design requirements from the very beginning of a project and allows the best compromise satisfying the specified constraints to be reached. The principal target is to reduce the design-cycle-time quite drastically, and to enable the designers to perform conceptual studies for any desired ranges of design parameters whilst maintaining the highest level of design quality and reliability.
Regarding fine-tuning in the final design stage, hitherto the benefits taken from advances in computational fluid dynamic (CFD) to boost the stage efficiency are quite significant. The improvements were, however, mainly achieved in the standard aerodynamic flow path design to the point where further potential for efficiency improvement on such issues seems to be relatively small. However, as part of continuing technological advance towards the design of new generations of highly efficient turbines, significant efforts have to be concentrated on a number of design

details on components placed outside the standard blading flow channel where still some room is left for further efficiency improvement.
In this paper, a brief discussion on the employment of high quality design technology used in the various phases of recent meridional flow path and blading optimization of high pressure and intermediate pressure cylinder (HP and IP) is given. Further, as part of design improvement efforts, the CFD modeling on components such as control-stage, wheel-chamber, design of the flow path in the extraction region, labyrinth leakage flow and leakage flow interaction with the mainstream are also described.

2 Conventional design aspects

2.1 Meridional flow path design (MFPD)

The meridional flow path is the most critical part of the overall turbine design which has direct bearing on each individual loss component generated from the turbine inlet to the outlet flange. In brief, the MFPD strongly impacts the blading design and the global turbine efficiency. For a given overall thermodynamic condition, mass flow rate and rotational speed, the MFPD of a given turbine frame makes use of an advanced technology with an integrated expert system which is comprised of the following elements (Figure 1):

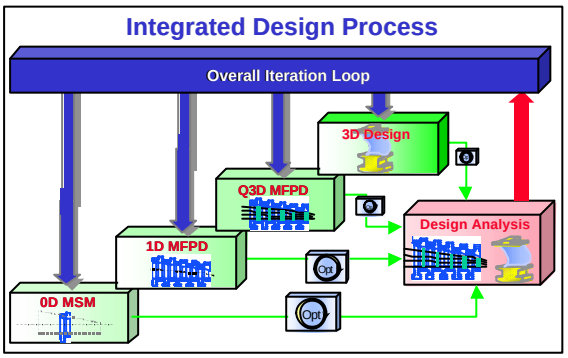

Figure 1: Integrated design system

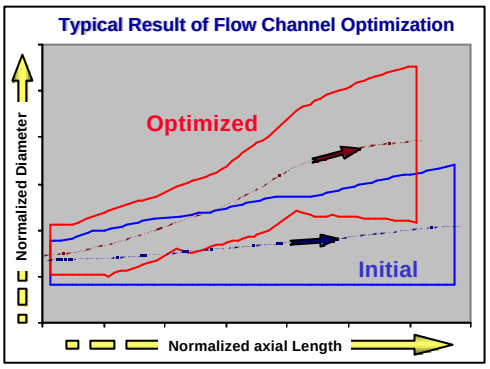

Fig. 2: Initial and optimized flow path

0D optimization: A global optimization under constraints which decides on the best choice of the overall averaged turbine key design parameters such as number of stages (Z), mean diameter (D_m), stage loading (μ), flow coefficient (ν), stage degree of reaction (R). These parameters are optimized for a single stage, operating under repeating stage condition, which represents the entire turbine (**M**ean **S**tage **M**odel - MSM).

1D optimization: Based on the results of the MSM algorithm, i.e. the above key design parameters being held fixed for a hypothetical middle stage, the MFPD continues with a 1D optimization program through which the inner and outer contours of the flow path are designed (Figure 2). During this step, the program has to decide upon the best distribution of the above mentioned design parameters in the axial direction without causing any geometrical or thermodynamic mismatching while moving from one stage to the next (constraint optimization).

Quasi-Three-Dimensional (Q3D) through flow optimization: In the course of Q3D optimization the best combination of appropriate vortex design {1}, blade lean configuration and details of meridional contour (end-wall contouring) is determined. One major qualitative design goal here is to achieve flow uniformity (uniformity of total pressure and mass flow density) in the radial direction at the exit plane of each stator and rotor, and convenient level of degree of reaction at the hub and tip sections (Figure 3). The latter is reached by finding the best combination of twist and tangential lean in the stator and rotor blades.

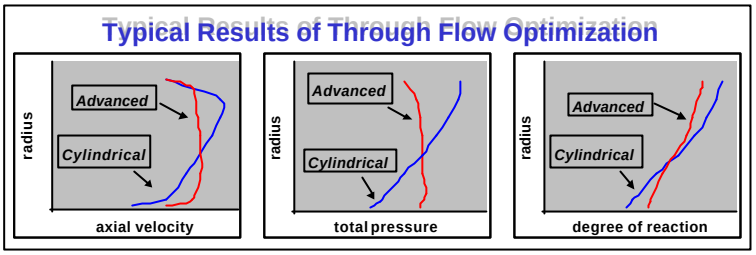

Figure 3: Typical results of through flow optimization

3D optimization: This design phase is of particular importance for design of the blade rows with pronounced secondary flow, which makes the flow strongly three-dimensional. Furthermore, the profile sections at the end-walls have to be further improved to account for the combined effects of secondary flow and leakage flow interaction at these locations. The Q3D design is, therefore, purely considered to be a good starting point for subsequent 3D optimization. This approach allows saving of numerous unnecessary and costly 3D iterations in the beginning of the design where many design alternatives have to be tried.

Following the above optimization process, the best feasible design is determined, i.e. the design satisfying the prescribed constraints, which minimizes the objective function (Fitness) defined as:

$$F = \sum L_i \times \sum C_i \times \prod P_i$$

Where, the first term stands for the sum of loss components, the second term is the sum of costs which reflect the cost contribution from blading, shaft and casing. The third term depicts the penalty function, which takes appropriate values depending on the degree of fulfillment of each of the specified constraints.

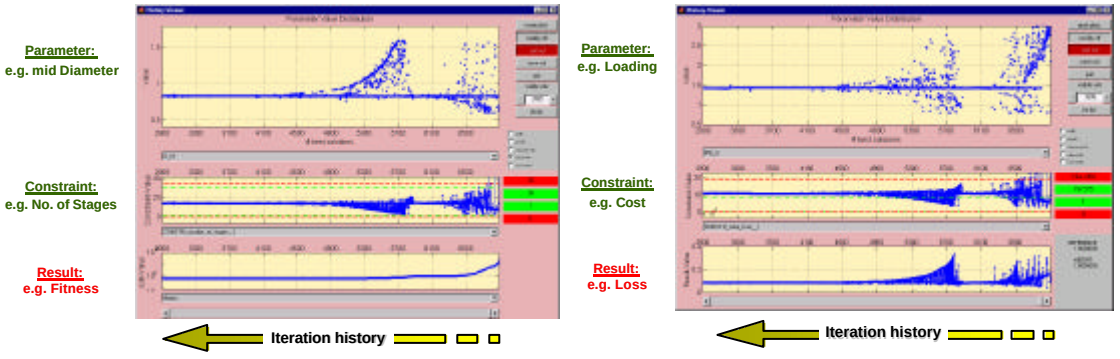

Figure 4: Convergence histories for a typical stage design optimization

Availability of a well proven loss correlation which can be applied through the whole design space, reliable modules for mechanical computations, a comprehensive cost

assessment routine, and careful definition of design constraints are of vital importance for the success of the above design steps. Extensive experience of the author's company, covering all possible types of axial turbine technologies, has made establishment of such correlations possible. Figure 4 (left part) shows typical optimization convergence history for the cases where number of stages is held as constraint and the evolution of fitness value (objective function) is shown as the result. On the right hand side of Figure 4 evolution of total cost, for the same design case during the above optimization is illustrated. Optimization algorithm routinely used in the design applications, rely on a combination of evolutionary and gradient algorithm. This allows to localize, in the first step, promising combinations of design parameters, and in the next step these solutions are used as starting point for the gradient algorithm in an attempt to reach the best solution (near absolute maximum).
Typical turn-around-time for each of the above-mentioned optimization steps, depending on the number of imposed constraints and complexity of optimization level, may require 0.5 to 12 hour of computation time on a highly paralleled and integrated UNIX work station net-work and power PC's.

2.2 Blading design

The main objective pursued in the initial blade design phase is to achieve the lowest local profile loss obtained on a Q3D basis. Practice guidelines based on well-established design criteria pertaining to geometric / aerodynamic details of profile in cascade are as integrated part of this design step {1}. The initial profile sections, designed on the basis of Q3D flow field, have to be subsequently checked and when justified improved via a three-dimensional (3D) optimization process.

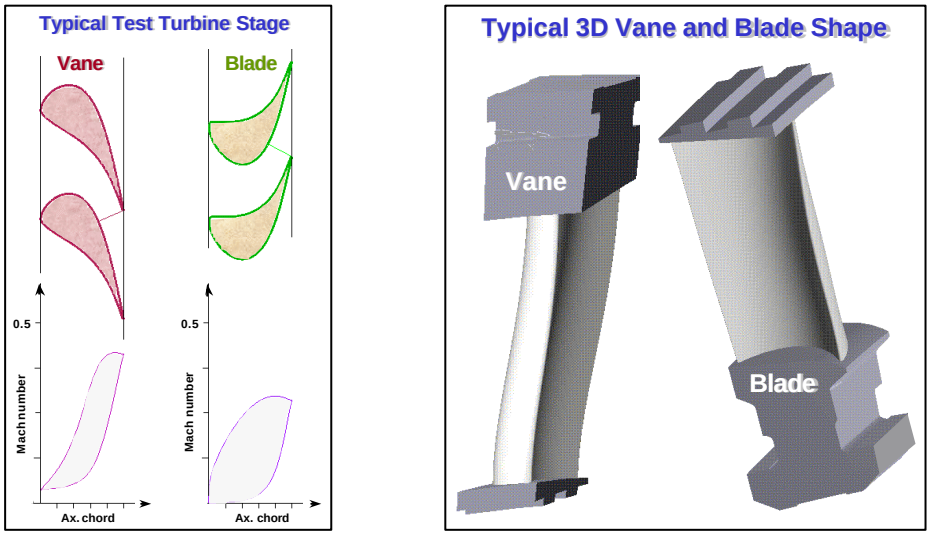

Figure 5: Example of typical low and high discharge angle blading

Figure 5 shows a typical highly loaded stator blade section with low discharge angle designed for front stages of HP cylinder with axial flow entry condition. The necessary moment of inertia of the section has been reached by judicious thickening of the profile whilst, compared to conventional blading, the chord length of the profile is very slightly increased. Such a design strategy allows the blade height / chord length (h/s) to be kept at a higher level, which is of paramount importance for secondary loss reduction. Additional key design issue is pitch / chord ratio (t/s) for optimization of which conflicting requirements on profile, secondary losses, unsteady losses and

part-count reduction have to be accounted for. The corresponding surface Mach number distribution indicates, despite a high degree of aft loading, low diffusion level on the rear part of suction side. Additional features of this design concern high incidence range required for efficient behavior at part load operation or to accommodate for other types of inlet flow non-uniformities, which may appear during normal operation. Figure 5 illustrate, additionally, a typical high-turning rotor section, which has been developed with the new design technology program system. The resulting 3D blade surfaces obtained by a 3D optimized profile section-stacking scheme are also shown.
Currently, experimental verification on a two-stage test turbine, which has been designed by making use of the new design technology, is ongoing.

3 Component design aspects

3.1 Turbine inlet ducts

The choice of the inlet ducts of turbine cylinders depends on the size of the turbine, requirements of the network and thereby the prescribed operating mode and economic considerations {2}. The impulse type control stage with partial arc admission (for HP cylinders) and sequential valve opening together with the scroll shaped inlet duct with radial-axial first stage (for HP, IP and LP cylinders) are the most commonly used type of inlet ducts.
Limitations on the admissible dimensions (compactness), control of loss generation and flow uniformity for the downstream blade row are among the major global considerations in the turbine inlet design process. In addition, in view of their shape complexities and the highly unsteady nature of the involved flow, careful attention has to be given to limit the degree of flow non-uniformities and hence to minimize the vibratory and thermal fatigue stresses in the downstream blade rows. During the last two decades, establishment of reliable design rules has been predominantly based on the results of sustained experimental measurements on model turbines {7} supplemented with a limited number of CFD modeling.

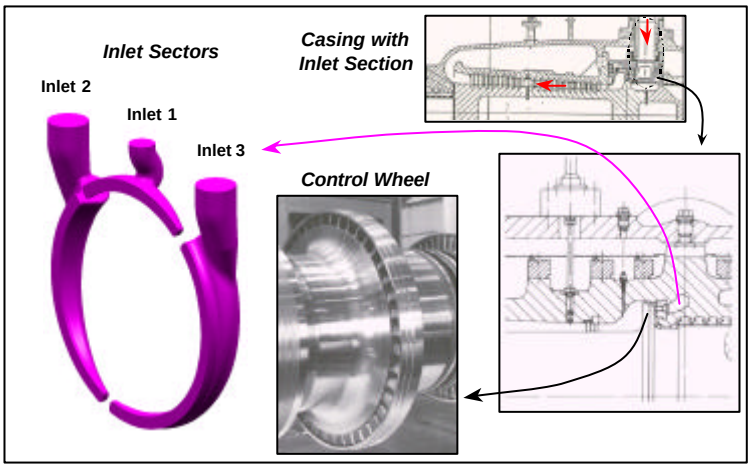

Figure 6a: Meridional sections and 3D views of a typical control stage

Control stage analysis: Figure 6a illustrates a 3D view of a typical control stage with 3 arcs of admission. The computational mesh (Figure 6b) for the control stage, which includes the full (360°) circular arc at mid-height, for 2D viscous unsteady computations with the nozzle box 2 opened i.e. load point 2 (LP2 corresponding to

about 40% admission rate) whereas, nozzle box 1 and 3 are closed. The modeling entails a multi-block mesh structure with 200000 mesh points. Careful trial computations have shown the adequacy of the above mesh resolution to capture the unsteady flow phenomena involved in the control stage. The computations were run with the perfect gas assumptions for steam as the working medium. Convergence (unsteady periodic solution) was reached following 5415 iterations. Note that each 32 time steps corresponds to one nozzle pitch and the required computation time for a converged solution was about 500h on a Risc work station.

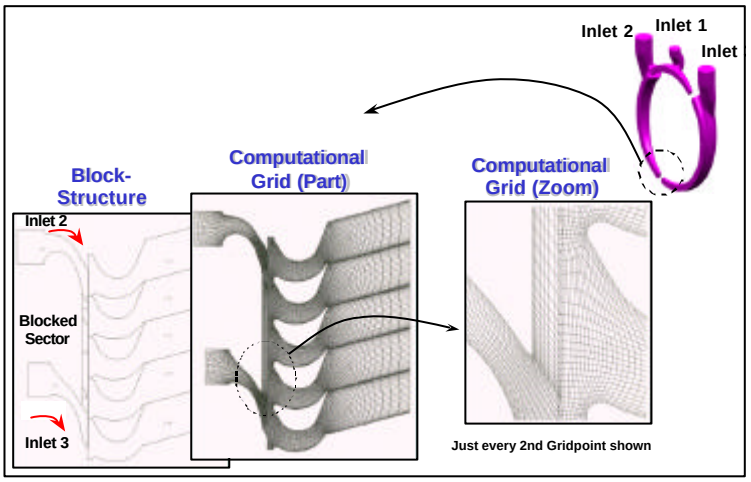

Figure 6b: Computational mesh, at mid height of the control stage

Figure 7a indicates that the first 2 rotor blades entering from the blocked sector (inlet 1) into the opened arc (inlet 2), feature severe flow separation. On the basis of the sufficient length of the admitted arc, the flow in the central part of the latter show similar behavior as classical stator-rotor interaction (wake convection, potential interaction) hardly influenced by the unsteadiness caused by blocked sector.
As expected {5,6}, patches of strong local supersonic flow was generated in the gap between the blocked sector and rotor blade, i.e. when the rotor leaves the arc of admission, which is opened (arc 2) and enters into the blocked sector, generating high losses. On the other hand, at the point where the rotor blade moves from the blocked sector into the opened arc, on the basis of higher local downstream blockage, the first stator adjacent to the blocked sector experience a higher Mach number level.

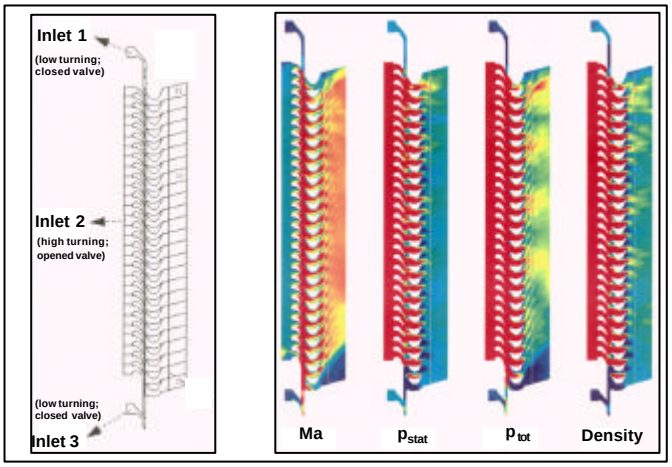

Figure 7a: Contour plots of Mach n°, static & total pressure, and density

Figure 7b depicts the unsteady axial and tangential aerodynamic forces of four successive rotor blades. Notice the rapid loading / unloading cycle (shock forces on the blades) when the rotor blade enters / leaves the arc of admission and the ensuing transient aerodynamic peak forces. The low amplitude undulation can be attributed to the interaction of the upstream nozzle wake with the rotor blades.

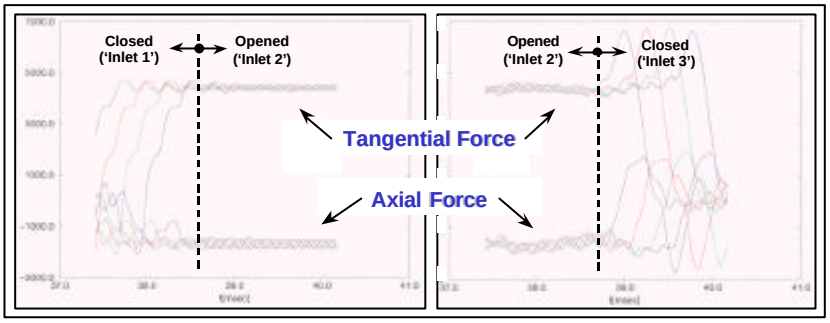

Figure 7b: Unsteady aerodynamic forces on the rotor blades

Intensive development work has to be done to define practical design measures, which alleviate excessive loss generation due to high local Mach number. This includes concurrent optimization of axial spacing, employment of tangential contouring on the blocked sector and development of advanced profile sections. In addition, changing the admission rate through the control stage normally lead to a huge variation of aerodynamic flow conditions and loading. Therefore, optimization of the control stage has to be necessarily based on a careful multi-design-point optimization scheme with special emphasis on mechanical and manufacturing requirements.

Wheel chamber analysis: The wheel chamber is designed to make the highly three-dimensional and non-uniform flow, coming out of the control stage, more uniform for the downstream blade rows. Experience shows that the control stage induced flow non-uniformity has a strong influence on the efficiency of the downstream stages. The decay or equalization of such flow non-uniformity strongly depends on the amount of swirl present in the flow and the shaping of the crossover duct. Measurement on a four-stage turbine {3} showed, that for a given admission rate, the tangential non-uniformities typically prevails in the first, second and third stages operating downstream of the control stage.

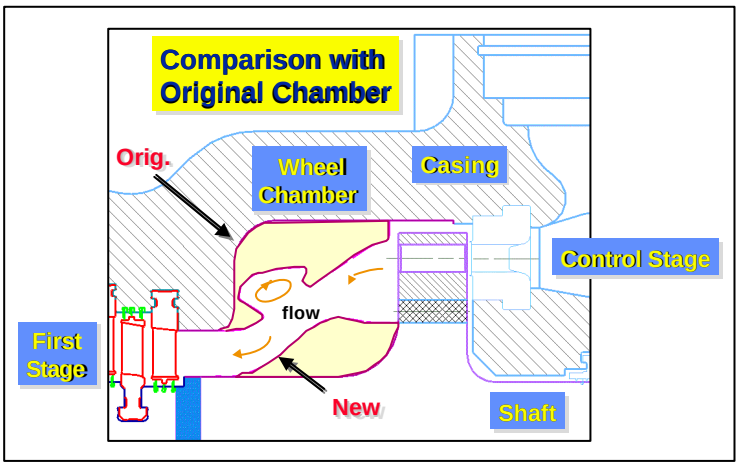

Figure 8a: Meridional section of the existing and new crossover duct

Figure 8a shows the meridional section of a typical crossover duct, which provides a sudden enlargement of the flow section at the exit of the control stage. Following sufficient axial length, through a 90° bend the flow path is brought to a lower radius with a narrowed annulus section leading to the stator inlet of the downstream stage. An alternative advanced design, which includes a bulge shaped cavity in the outer contour, is designed to:
a) Enhance the flow uniformity, b) reduce the incurred losses, c) reduce tip leakage loss in the control wheel and d) provide optimum flow guidance in the duct.
The CFD modeling for both duct configurations was based on 3D-viscous computations (TASCflow). Numerous simulation were run with differing boundary conditions. The inlet conditions were defined by combining the 3D radial distributions obtained from 3D-steady and 2D-unsteady computations on the upstream control stage (see the above section). Four 3D runs were performed, three of which with the inlet boundary conditions taken at three different time instants obtained from the 2D-unsteady computations, and one run with the time averaged conditions. At the duct outlet, porous medium conditions was adjusted and set to simulate the presence of the downstream blade row. This study has indicated, that the design studies of the crossover duct can be performed, by making use of the time-averaged boundary conditions.
Notice that the flow in the existing duct is characterized by two large-scale vortices located in the lower and upper corner of the duct (Figure 8b). The momentum exchange of the main flow with the lower vortex is principally through shear layer, which is little affected by the level of swirl velocity component. Consequently, the role of the lower vortex is predominantly to produce loss than to contribute to the uniformity of the downstream flow. The strength of the upper vortex and the corresponding dissipation through this vortex, however, changes quite significantly (streamline centripetal acceleration) with the amount of swirl velocity component present in the main flow. Therefore, the upper vortex plays a predominant role in the flow equalization process especially at part load operating conditions where swirl velocity component is very high. The main goal in the design of the new duct was to reach a refined configuration, which give rise to a substantial reduction of the size of the lower vortex. This combined with the requirement on the optimum flow guidance has led to the development of the new crossover channel.
Furthermore, additional blockage provided by the new duct, in the tip region of the rotor exit plane has reduced the leakage flow by about 20%. This effect is evidenced, in the new design by the two new small vortices in the tip region of the duct inlet plane (Figure 8b).

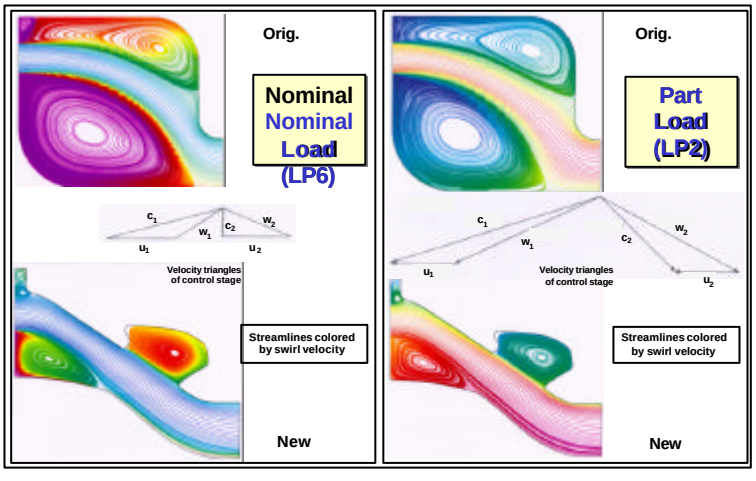

Figure8b: Streamline pattern (colored with swirl velocity)

Note that the bulge shaped cavity can act as a Helmholz resonator the frequency of which depends on the width of the cavity opening and the volume of the cavity. Exploratory checks were done to ensure that the eigenfrequency of the cavity does not coincide with the eigenfrequency of the duct and lies well above that of the downstream rotor.
Further, manufacturing constraints for welding of the eroded control wheel on the turbine shaft, availability of minimum space for welding process and mechanical considerations has dictated the minimum size of the lower vortex.
Figure 8c compares spanwise (tangentially averaged) variation of the axial velocity and static pressure of the existing and the new crossover duct which is representative for both part and full-load operating conditions. From these figures, it can be concluded that the flow uniformity at the duct exit has been improved. As regards loss generation in the duct, the new design, as expected, gives rise to a significantly lower loss level compared to the old design.
The future design improvement / check must include unsteady computations including the upstream control stage and the downstream rotor blade row.

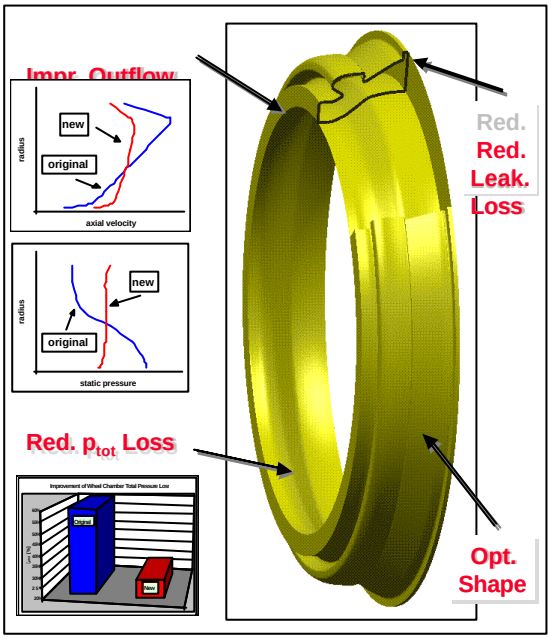

Figure 8c: Spanwise variation of axial velocity and static pressure

Inlet Spiral, radial-axial stage: Figure 9a shows the modeling of the scroll-shaped inlet duct of a typical intermediate pressure (IP) cylinder. A variety of CFD computations were conducted which include inlet spiral alone, inlet spiral with porous medium imposed at the outlet to simulate the downstream radial row and inlet spiral implicitly coupled with the downstream stage. Such computations revealed that the flow in the exit plane of the crossover duct is strongly non-uniform in the radial direction. To improve this situation, the crossover duct has been extended axially to provide more time to the flow to mix-out and become more uniform. This solution is found to be insufficient and led to a slight increase of the overall loss on the basis of increased wetted area. Two additional design changes were introduced:

a) the inlet spiral was redesigned with an eccentric flow sections which allows maintaining the original machine axial length,
b) introduction of endwall contouring, on the hub and casing to utilize streamline curvature effect and reduce radial non-uniformities.

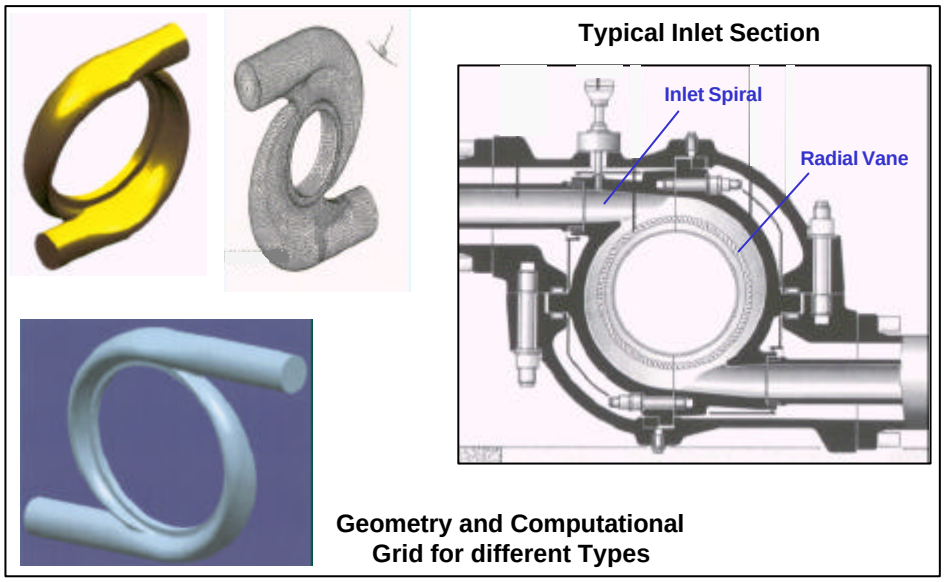

Figure 9a: 3D view and computational mesh of the inlet spiral

Figure 9b illustrates the layout of the new crossover duct. The design optimization of the scroll and downstream stage-crossover-duct has been based on fully viscous 3D approach.

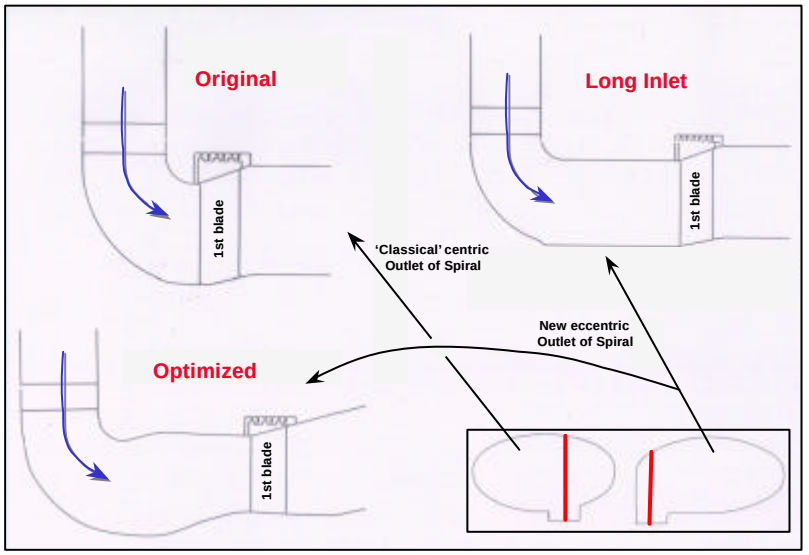

Figure 9b: Meridional section of the existing and optimized crossover duct

From Figure 9c, the above-mentioned improvement in flow uniformity at the inlet of the first rotor blade can be clearly seen. The relative inlet angle at the hub section has been drastically reduced (≈14°). Through this and the resulting increase of kinetic energy in the axial direction, the intensity of cross flow and the ensuing secondary loss growth are decreased markedly. To ensure identical throat area, the hub diameter of the rotor has to be arranged with a small amount of negative flare angle. This constitutes a minor drawback of the present design, which results in a slight deterioration of flow uniformity at the rotor exit.

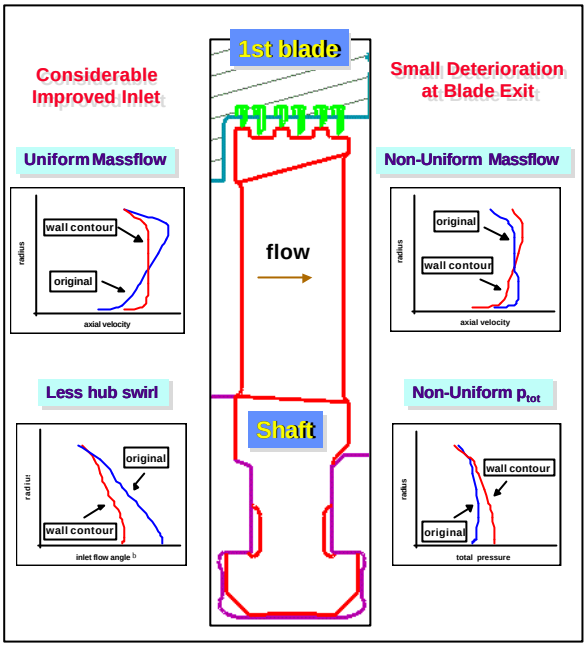

Figure 9c: Aero-thermodynamic state at inlet / exit of first rotor

3.2 Casing contour in the bleeding zone

To investigate the flow structure in the bleeding zone, 3D viscous stage computations rotor-stator (mixing-plane and frozen rotor) with bleeding in between have been done for the expected operating conditions (several extraction rates down to zero). The behavior of the rotor-tip-leakage re-entry flow in the bleeding zone is one of the main focuses of this computation. It can be seen that the jet of leakage from the last labyrinth strip produces a sizable region of separated and back flow in the casing region (Figure 10). Under this circumstances, not only high local losses is produced, but also the ensuing blockage makes the extracted flow to accelerate locally to high velocity levels which further enhance entropy generation.

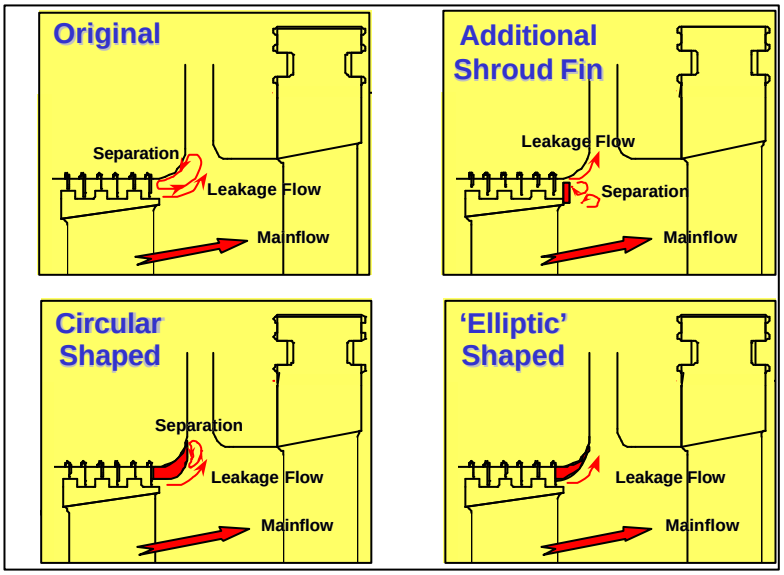

Figure 10: Illustration of design improvement in the tip regions of bleeding zone

A variety of new designs were suggested, modeled and assessed. The optimized configuration feature an elliptic type contouring matched to the casing region behind the last strip. This improved casing contour in the bleeding region avoids such a large-scale flow separation and entropy production.

3.3 Labyrinth seals - Leakage flow interaction

Leakage flow aerodynamics has particular significance in the design process of reaction blading. Compared to a low reaction design, higher leaking diameter at the hub section of the stator and higher level of degree of reaction at the rotor tip section, makes the relative portion of the leakage mass flow and the ensuing leakage loss significantly higher. Under such conditions, considerations on labyrinth seal layout optimization to reduce leakage mass flow, and arrangement of reentry flow geometry to control interaction losses with the mainstream flow, gain considerable importance. The impact of leakage flow on the radial position and strength of secondary flow is qualitatively illustrated in Figure 11a.
Figure 11b shows the surface Mach number distribution at the rotor hub section for zero and finite value of radial clearance. It can be seen that leakage flow gives rise to a considerable local negative incidence. Similar phenomenon happens at the stator tip section where rotor tip leakage impinges on the downstream stator tip section {1}.

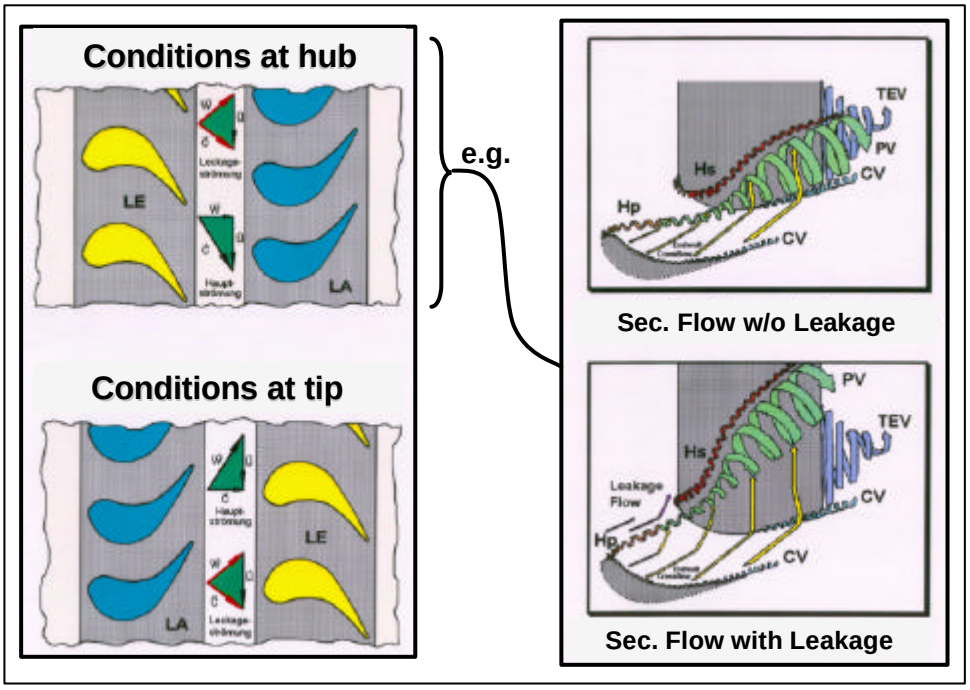

Figure 11a: Impact of leakage flow on the endwall flow structures {1}

To minimize interaction losses, comprehensive investigations were carried out to optimize the re-entry geometry of the leakage flow (endwall contouring) {1}. Such contouring allows the leaking flow to re-enter the mainstream with a minimum of perturbation or entropy production. In addition to comprehensive CFD modeling (Figure 11c), the subject of leakage interaction in reaction blading environment is currently under investigation through FVV and AG-Turbo projects.

4 Conclusions

This paper shows how modern design systems based on CFD and optimization strategies can be used for major improvements in the overall efficiency of a steam turbine. Attentions were concentrated to a number of specific sources of losses besides standard blading flow channel and possible solutions were suggested to decrease them.

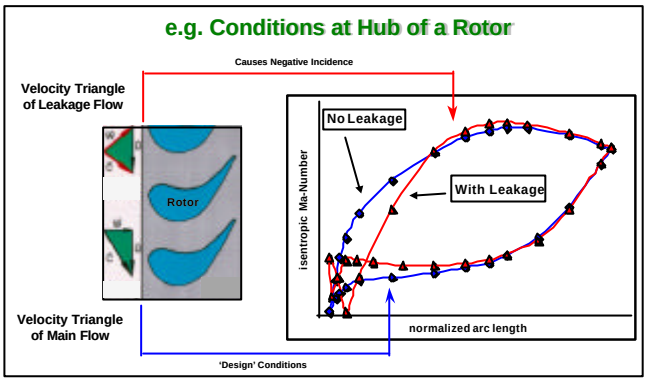

Figure 11b: Impact of leakage flow on local surface Mach number

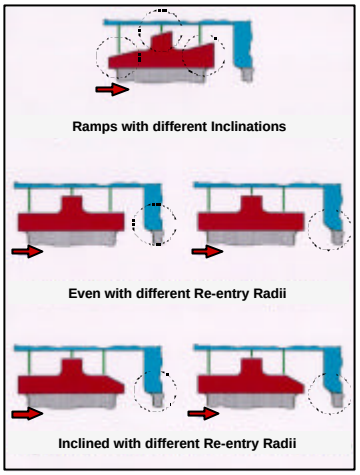

Figure 11c: Re-entry geometries

Acknowledgements

The authors would like to thank the involved co-workers of the departments: ZXF, CHCRC-T2, KWS57, KWBS67, and KWBS21. Especial thanks are extended to the authorities of ABB Alstom Power for giving permission to publish this paper.

List of references

1. Havakechian, S., Greim, R., “Aerodynamic Design of 50 per cent Reaction Steam Turbine Stages” Proceedings of IMechE, J. of Mechanical engineering Science part C vol. 213, pg. 1-25
2. ABB Power Generation, “Sliding and Constant Pressure Operation in Reheat Power Plants”, HTGD A51018E / Index B
3. Bohn, J., Ziemann, M., “Einfluss der Überströmgehäusegeometrie auf den Strömungsausgleich bei Turbinen mit Teilbeaufschlagung”, VGB Kraftwerk-technik 2/98
4. Immich, H., Inlet Scroll for low-pressure steam turbine with radial stationary blades, ASME, Aerothermodynamics of Steam Turbines, 1981
5. J Skopek, J Vomela, Ltajc, J Polansky, “ “Partial Steam Admission in an Axial Turbine Stage”, ImechE 1999 C557 / 077
6. He L., “Three-Dimensional Unsteady Navier-Stokes Analysis of Stator-Rotor Interaction in Axial-Flow Turbines”, IMechE 1999, C557/049
7. FVV, “Verlustquellen und Strömungsausgleich in teilbeaufschlagten Turbinenstufen”, “Überstömgehause teilbeaufschlagter Turbinen”, “Untersuchung des Strömungsausgleiches in den Schaufelreihen ungleichförmig angeströmter Turbomaschinen”, “Sonden-/Schaufelinteraktion”. RWTH Aachen, seit 1985